ELSEVIER

Contents lists available at ScienceDirect

Brain Multiphysics

journal homepage: www.sciencedirect.com/journal/brain-multiphysics



Full Length Article

Revealing the heterogeneity of plasma protein and cognitive decline trajectory among Mild Cognitive Impairment patients by clustering of brain atrophy features

My Nguyen ^{a,b}, Bao Pham ^{b,c}, Toi Vo ^{b,c}, Huong Ha ^{b,c,*}

- ^a Faculty of Biology Biotechnology, University of Science, Ho Chi Minh City 70000, Vietnam
- ^b Vietnam National University Ho Chi Minh City, Ho Chi Minh City 70000, Vietnam
- ^c School of Biomedical Engineering, International University, Ho Chi Minh City 70000, Vietnam

ARTICLE INFO

Keywords: Alzheimer's disease Mild cognitive impairment Clustering analysis Brain atrophy Plasma protein Cognitive decline

ABSTRACT

Alzheimer's disease (AD) is suggested to be a heterogeneous disorder, but limited studies explore the heterogeneity of the Mild Cognitive Impairment (MCI) stage. This study aimed to tackle such problems using the CIMLR (Cancer Integration via Multikernel Learning) algorithm to cluster brain structural features extracted from T1weighted Magnetic Resonance Images of MCI patients from Alzheimer's Disease Neuroimaging Initiative. The demographic and cognitive results, characteristics of brain structural features, plasma biomarkers, and longitudinal cognitive trajectory were analyzed for each cluster. The CIMLR clustering analysis revealed four distinct clusters. Cluster 1 is the oldest group but has had mild atrophy and moderate progression with elevated Tumor Necrosis Factor Receptor 2 level; and low Brain-Derived Neurotrophic Factor and CD40 Ligand levels. Cluster 2 showed the highest risk for aggressive MCI progression, with abnormal Leptin, Adiponectin, and Creatine kinase-MB values. Cluster 3 exhibited a low level of Monokine Induced by Gamma Interferon and mild atrophy that shared similar patterns with Cluster 1. Cluster 4 represented the healthiest group during longitudinal tracking, with the mildest Parahippocampal atrophy, which was found to be positively correlated with cognitive impairment and amino acid levels. The longitudinal analyses showed the potential of Hepatocyte Growth Factor as a marker for slow cognitive impairment; Cortisol and Neurofilament Light Polypeptide as prognosis markers for aggressive MCI progression. These findings may lay out new suggestions for further research contributing to the accurate diagnosis and precision medicine for dementia and AD.

1. Introduction

Alzheimer's Disease (AD) is a heterogeneous disorder with high diversity in demographics, progressive rate, brain atrophy phenotypes, and other characteristics [1–6]. It is crucial to acknowledge that current treatments are unable to reverse brain atrophy in the advanced stage of AD. Therefore, understanding the heterogeneity at the early stage of the disease, known as Mild Cognitive Impairment (MCI), can help to facilitate the drug development process and establish improved disease management strategies for the patients.

In studying heterogeneity using computational methods, cluster analysis is widely used; however, it has certain limitations when applied to investigating AD characteristics. Firstly, there is a scarcity of studies that have examined the heterogeneous characteristics of the MCI population, with most research focusing on the AD stage [2,7-9]. Secondly, most clustering studies analyzed the heterogeneity in three types of patients simultaneously: the cognitively normal, MCI, and AD patients [10–13]. Consequently, the resulting clusters comprise individuals from all three groups, making it challenging to identify unique characteristics specific to the early stages of disease development and the potential development of diagnostic biomarkers. The third issue is that several studies investigating the heterogeneity of MCI encountered an excessive number of clusters, which hinders further characterization of each cluster [11]. Therefore, employing a new approach that can overcome mentioned limitations to study the MCI stage's heterogeneity effectively is crucial.

E-mail address: htthuong@hcmiu.edu.vn (H. Ha).

https://doi.org/10.1016/j.brain.2024.100093

^{*} Corresponding author at: School of Biomedical Engineering, International University (Vietnam National University – Ho Chi Minh City), Quarter 6, Linh Trung Ward, Thu Duc, Ho Chi Minh City, Vietnam.

Clustering studies for AD commonly employ Magnetic Resonance Imaging (MRI) due to its rich and extensive data information. Specifically, MRI allows for visualizing the brain's structure at the voxel level, providing a clear representation of brain atrophy, indicative of a progressive neuronal loss in AD. This information provides insights into the heterogeneous patterns of atrophy observed in AD patients. Besides the structural brain imaging markers, most current clustering research on AD patients concentrated on studying protein markers derived from cerebrospinal fluid (CSF), including tau, phosphorylated-tau, and Beta-Amyloid (Aβ) [4,13,14]. These studies confirmed the heterogeneity of the proteins within AD patients; however, CSF proteins have limited clinical utility due to their high costs, invasiveness, need for well-trained practitioners for sample collection, and poor accessibility in remote areas. In contrast, blood-based biomarkers are promising alternatives due to their convenience in sample collection with minimal invasion, low cost, and high time effectiveness. Notably, by utilizing the clustering method on the plasma protein data of CN, MCI, and AD patients, blood-based proteins were suggested to be heterogeneous [15]. However, four clusters from the mentioned study still contain a mixture of three diagnostic groups of patients (CN, MCI, and AD), which is challenging to identify specific biomarkers for prognostic and early diagnosis. Therefore, it is crucial to explore the heterogeneity of plasma proteins, specifically among MCI patients, to gain a comprehensive understanding of this population. This knowledge will contribute to unraveling the underlying mechanisms related to heterogeneity and its relationship to brain atrophy patterns, proposing new insights and promising applicable biomarkers of high-risk populations.

Studying the heterogeneity of the mild cognitive impairment (MCI) population only at a single time point, usually at baseline, provides a limited view of the complex and varied trajectories of disease progression. Meanwhile, the longitudinal analysis enables capturing the longterm trends and progression of the disease and identifying the distinct characteristics of high-risk individuals with aggressive progression. Existing studies mostly categorized the MCI population into two subgroups: cMCI (converted-MCI who converted to AD within 36 months) and sMCI (stable-MCI who did not convert to AD within 36 months) [16]. However, this classification does not capture the full spectrum of disease progression, as evidenced by studies demonstrating varied patterns in cognitive performance, brain regions, and CSF protein across different patient groups [11,17]. This indicates the limitation of solely relying on cMCI and sMCI to represent high-risk populations adequately. Therefore, it is crucial to study the heterogeneity of MCI longitudinally. Additionally, current longitudinal studies on the heterogeneity of MCI mainly focused on cognitive declines, common brain regions such as the hippocampus, and common CSF biomarkersrs [4,14,18-21]. This limitation leads to the need to expand the scope of longitudinal analysis to changes in additional brain regions beyond the hippocampus and explore new biomarker variations such as plasma protein. This new way of research allows diving deeper into the relationship among those characteristics is essential for identifying new prognostic markers.

In this study, we aimed to apply an advanced clustering method to investigate the heterogeneity in the MCI stage using brain features extracted from MRIs at the baseline as the input data. Then, a multimodal analysis was conducted to identify the demographics, important brain characteristics, and plasma protein characteristics of each cluster at the baseline. Finally, to gain insights into the relationship between important brain characteristics, cognitive performance, and plasma protein levels, longitudinal analyses were applied to study the long-term changes. Our longitudinal analysis will track the changes in brain atrophy and cognitive function over 36 months, aiming to provide a comprehensive view of MCI progression and propose new biomarkers for prognosis.

2. Materials and methods

2.1. Data description

The data used for this study were retrieved from the Alzheimer's Disease Neuroimaging Initiative (ADNI), which is available at www. loni.ucla.edu/ADNI. ADNI is a common longitudinal and multi-site database for AD. It was launched in 2003 and led by Principal Investigator Michael W. Weiner, MD. The main goal of ADNI was to investigate the role of serial magnetic resonance imaging (MRI), positron emission tomography (PET), other biological markers, and clinical and neuropsychological assessment in studying the progression of mild cognitive impairment (MCI) and early Alzheimer's disease (AD).

2.1.1. Subjects

Subjects selected for this study had to be diagnosed as MCI at baseline and have their blood biomarker information and longitudinal information (MRI and cognitive scores) available on the ADNI database. The final data comprised 359 subjects with MCI at baseline, including 167 cMCI subjects and 192 sMCI subjects. The demographic information of the study cohort at baseline is summarized in Table 1.

2.1.2. MR images

Imaging data used in this study were the T1-weighted MR scans with the MP-RAGE sequences of MCI subjects from ADNI 1 and ADNI GO/2. These images were obtained at four different time points, including the baseline (the first visit of patients, with n=359), month 12th (n=317), month 24th (n=257), and month 36th (n=200). Various models of MR scanners were used for the MRI acquisition, and details of the acquisition protocol for the MRI data can be found on ADNI's website (http://adni.loni.usc.edu).

2.1.3. Plasma biomarkers

In the beginning, 234 plasma markers from four Biospecimen Dataset from ADNI were pre-selected for this study, including 190 plasma biomarkers, plasma NFL, plasma $A\beta$ proteins 40 and 42, and 41 amino acids. The methods and protocols used to measure these plasma markers are described in "Biomarkers Consortium Plasma Proteomics Project RBM Multiplex", "Blennow Lab ADNI1–2 Plasma neurofilament light (NFL) longitudinal (ADNI1, GO, 2)", "ADMC Duke Biocrates P180 Kit Ultra Performance Liquid Chromatography (ADNI1)", and "UPENN Plasma Biomarker Data" (available at http://adni.loni.ucla.edu). After removing missing values, the final sample comprised 191 plasma markers.

2.2. Study design

The overview of the study design is illustrated in Fig. 1. Firstly, the sMRIs of 359 MCI subjects are pre-processed with Freesurfer to extract 310 brain structural features (including 106 vol features, 68 area features, 68 thickness features, and 68 mean curvature features). Those 310 features are then normalized in the range from 0 to 1, which were the

Table 1 Demographic information of 359 MCI subjects recruited from ADNI. Data is illustrated as mean \pm standard deviation or number/number.

| | cMCI | sMCI | Total |
|---|--|--|--|
| N | 167 | 192 | 359 |
| Gender (M/F) | 101/66 | 128/64 | 229/130 |
| Age | 74.6 ± 7.5 | $\textbf{74.9} \pm \textbf{7}$ | $\textbf{74.8} \pm \textbf{7.3}$ |
| Education | 15.7 ± 2.9 | 15.5 ± 3.2 | 15.6 ± 3.1 |
| MMSE | 26.6 ± 1.7 | 27.3 ± 1.8 | 27 ± 1.8 |
| CDR | 0.5 | 0.5 | 0.5 |
| FAQ | 5.7 ± 5.1 | 2.5 ± 3.4 | 4 ± 4.5 |
| ADAS-Cog13 | 21.1 ± 6 | 17 ± 6.3 | 18.9 ± 6.5 |
| ApoE4 (+/-) | 112/55 | 87/105 | 199/160 |
| Education MMSE CDR FAQ ADAS-Cog13 | 15.7 ± 2.9 26.6 ± 1.7 0.5 5.7 ± 5.1 21.1 ± 6 | 15.5 ± 3.2 27.3 ± 1.8 0.5 2.5 ± 3.4 17 ± 6.3 | 15.6 ± 3.1 27 ± 1.8 0.5 4 ± 4.5 18.9 ± 6.5 |

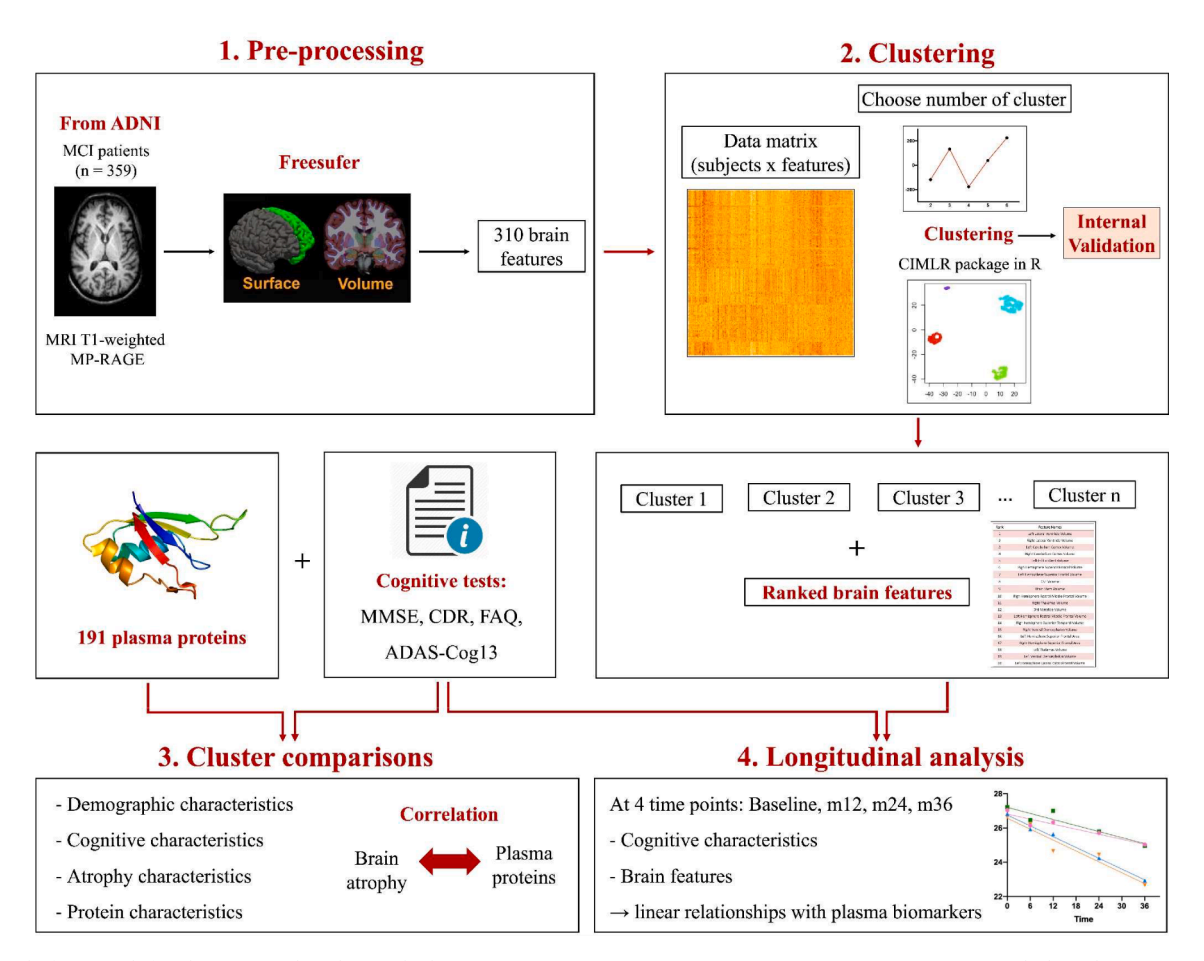


Fig. 1. A study framework for clustering and analyzing the heterogeneities in MCI patients. CIMLR = Cancer Integration via Multi-kernel Learning, MCI = Mild cognitive impairment, MMSE = Mini-Mental State Examination, CDR = Clinical Dementia Rating, FAQ = Functional Activities Questionnaire, ADAS-Cog = Alzheimer's Disease Assessment Scale-Cognitive Subscale test.

input data for the clustering step. These normalized features were combined with MCI subjects to create a n x m matrix, where n represents the MCI subjects, and m represents the brain features. The optimal number of clusters is determined by a heuristic method based on gap statistics, which is available in the CIMLR (Cancer Integration via Multikernel Learning) package in R [22]. Subsequently, the data matrix was analyzed by the CIMLR algorithm and clustered into subgroups. The algorithm also exported a list of structural features ranking based on their contribution to the clustering analysis. Thirdly, comparisons among clusters were done using the top 20 ranked brain features from the clustering result, plasma biomarkers, and cognitive scores. The correlation tests were conducted to investigate the relationship between brain atrophy and plasma proteins. Finally, there was a longitudinal analysis to track the changes in cognitive characteristics, brain atrophy within 36 months and their linear relationships. Moreover, linear relationships between cognitive trajectories and plasma biomarkers also were analyzed.

2.2.1. Data pre-processing

All the MR images in this study were reconstructed and segmented by Freesurfer version 5.3 ("recon-all"), which is documented at http://surfer.nmr.mgh.harvard.edu. Freesurfer is an open-source software that analyzes the functions, connectivity, and structures of the human brain, allowing the extraction of brain imaging features. The processing procedure of the software is described in detail in [23,24]. In this study, after undergoing pre-processing, 358 brain structural features were extracted using Freesurfer. To focus specifically on characterizing atrophy in individual brain regions, whole-brain and general features

were excluded. Therefore, the final selection comprised 310 structural features, encompassing 106 vol, 68 area, 68 thickness, and 68 mean curvature of brain regions based on Freesurfer's default atlas. The complete list of the selected brain features can be found in the **Supplementary File 1**. Then, 310 features are normalized to make all data have the same range from 0 to 1. These 310 normalized features were used as input for the CIMLR model.

2.2.2. Clustering method

CIMLR is an extended clustering method of the SIMLR (Single-cell Interpretation via Multi-kernel LeaRning) algorithm [25]. This algorithm was chosen to be implemented due to its ability to handle large amounts of data, good performance on a variety of datasets, especially for highly heterogeneous data, and interpretable results [22]. The detailed description of CIMLR is mentioned in [22].

In general, CIMLR is based on the multi-kernel learning method, which combines kernels for each feature to determine how similar each pair of patients is [22]. 310 normalized brain features extracted from sMRI at baseline by Freesurfer were used for the CIMLR clustering step. The input data, formated as a matrix of N subjects x M brain features, was used to construct a series of Gaussian kernels, which are defined below:

$$K(x_i, x_j) = \frac{1}{\epsilon_{ij}\sqrt{2\pi}} \exp\left(-\frac{\|x_i - x_j\|_2^2}{2\epsilon_{ij}^2}\right)$$

With x_i and x_j are respectively the ith and jth rows of the input data and ϵ_{ii}^2 is the variance.

Similarly to [22], the optimization problem using Gaussian kernels

to build one subject x subject similarity matrix:

$$min_{S,L,w} - \sum_{i,j,l} w_l K_l(x_i, x_j) S_{ij} + \beta ||S||_F^2 + \gamma tr(L^T(I_N - S)L) + \rho \sum_l w_l \log w_l$$

subject to
$$L^TL = I_C, \sum_l w_l = 1, w_l \geq 0, \sum_i S_{ij} = 1, \text{ and } S_{ij} \geq 0.$$

Here, N is the number of subjects, and C is the number of clusters. i, j, and l denote the row (subject), the column (brain feature), and the kernel index. S represents the similarity matrix, w_l is the weight of each Gaussian kernel, I_N and I_C denote the NxN and CxC identity matrices, β and γ are tuning parameters, tr denotes the trace of the matrix, $||S||_F$ stands for the Frobenius norm of S, and L is a matrix enforcing C clusters on S.

Each kernel is a measure of patient-to-patient distance, and CIMLR learns weights for multiple kernels. Consequently, it combines the multiple kernels into a symmetric similarity matrix with C blocks, with each block being a set of MCI patients who are highly similar to each other. In other words, each block is a cluster and C is the number of determined clusters. The number of clusters C has to be determined beforehand by a heuristic method [22,25,26]. This method was based on the eigenvalues of the Laplacian matrix and the gap statistics approach [22,25,26].

Finding an indicator matrix Z(R) = XR for a given value of C is the goal. X is the matrix of the top eigenvectors of the similarity Laplacian, and R is a rotation matrix.

$$M[(R)]_i = max_j[Z(R)]_{i,j}$$

The cost function to be minimized:

$$J(R) = \sum_{i,j} \frac{[Z(R)]_{i,j}^{2}}{[M(R)]_{i}^{2}}$$

The most optimal number of clusters in CIMLR shows the most significant drop over the set values of C [22,25,26]. In this study, the range value of C is 2 - 10 clusters. Subsequently, the similarity matrix is used for dimension reduction by applying t-distributed stochastic neighbor embedding (t-SNE) and then clustering into subgroups by K-means [27].

Features were ranked based on their importance for clustering by the Laplacian Score method to measure the contribution of each feature to the above similarity matrix. The feature scores were then aggregated by the Robust Rank Aggregate method and the final features ranking list was exported based on p-values for the features ordered by significance. The clustering analysis was performed with R version 4.1.1 using the CIMLR package (installing and codebase information, including estimating the number of clusters, CIMLR clustering, and feature ranking can be found at https://github.com/danro9685/CIMLR).

2.2.3. Cluster validation

This study used four validation methods to assess the clustering results: Davies-Bouldin, Silhouette, Pakhira-Bandyopadhyay-Maulik (PBM), and Ray-Turi indices [28–31]. These methods serve as internal validation by comparing the stability of the clustering results across different C values of clusters and with other clustering algorithms. The four most common clustering algorithms: K-Means, Hierarchical clustering, Partition Around Medoids (PAM), and Clustering Large Applications (CLARA), were chosen to compare.

The Silhouette Index determines the separation distance between clusters using the mean intra-cluster distance and the mean nearest-cluster distance [29]. The PBM index is calculated using the distances between the data points and their barycenters and the distances between the barycenters themselves [30]. Thus, higher values for the Silhouette and PBM indices suggest more stable clustering results [29,30].

The Davies-Bouldin index represents the average similarity measure between each cluster and its most similar cluster, where the ratio of within-cluster distances to between-cluster distances determines similarity [28]. Lower scores reflect clusters that are more distant and less dispersed. The Ray-Turi index calculates the mean squared distances of all data points relative to the cluster's barycenter, considering the minimum squared distances between all cluster barycenters [31]. Therefore, lower values of the Davies-Bouldin and Ray-Turi indices indicate more stable clustering results [28,31].

2.3. Cluster comparison

The main goal of this analysis is to identify the unique characteristics of each cluster. To be more specific, the following characteristics were compared between each cluster and the rest of the population: (1) Demography: Number of subjects (including the number of cMCI and sMCI patients), gender ratios, age, years of education, and percentage of people carrying APOE4 alleles; (2) Cognitive measurements: Baseline values of MMSE, CDR, FAQ, and ADAS-Cog13; (3) Brain atrophy: From a list of 310 brain structural features, the top 20 ranked features as suggested by CIMLR were analyzed. This selection was based on the rationale that a comprehensive analysis of all 310 features would be time-intensive and beyond the scope of this study; and (4) Plasma biomarkers: 191 plasma proteins and amino acids. The reason that only focus on the top 20 is because it would take considerable time and effort required to analyze all 310 features comprehensively. Next, the correlation between the top 20 ranked brain regions and plasma biomarkers was then performed by Spearman correlation function from SciPy Library (the p-values of the correlation tests were corrected by the Holm-Bonferroni method).

2.4. Longitudinal analysis

The longitudinal analysis was performed in order to track changes and trends in the progression of MCI in each cluster from baseline to the follow-up 36 months. There are two main types of input data in the longitudinal analysis. Firstly, four cognitive tests (MMSE, CDR, FAQ, and ADAS-Cog13) of 359 subjects at five different time points: baseline, month 6, month 12, month 24, and month 36 were obtained. Secondly, MRI data of the same 359 subjects were collected at baseline, month 6, month 12, month 24, and month 36. These MR scans were pre-processed to obtain the top 20 ranked brain features for longitudinal analysis. These two types of data were input to the Simple linear regression at five time points (baseline, month 6, month 12, month 24, and month 36). From here, the best-fit slope values were extracted to evaluate the progression of MCI in each cluster over the 36 months in terms of cognitive performance and brain atrophy.

Additionally, linear regression was also applied to investigate whether baseline values of plasma proteins and brain features at baseline could be indicative of cognitive trajectories over 36 months. This linear regression involved correlating the delta (change) in cognitive test scores (MMSE, CDR, FAQ, and ADAS-Cog13) from baseline to 36 months with the baseline plasma protein levels and brain features.

The longitudinal analysis was conducted by the Simple linear regression tool in GraphPad Prism Software version 8.3.1. Only linear relationships having p-value < 0.05 were chosen to be represented by GraphPad Prism. Missing values of each feature were handled by the pairwise deletion method in the longitudinal analysis.

2.5. Statistical comparison

All statistical comparisons in this study, including the demographic, cognitive measurements, brain atrophy, and plasma biomarkers comparisons were performed in R version 4.1.1. For the clinical and cognitive characteristics comparisons, Chi-squared test and Kruskal–Wallis test were used to analyze differences among means of clusters. Moreover, the non-parametric Mann-Whitney-Wilcoxon tests were performed to compare the brain atrophy and plasma protein characteristics between each cluster and the rest of the population. The comparisons

between each cluster were performed by Kruskal–Wallis test followed by Dunn's post-hoc analysis. All the p-values for multiple testing in this study were corrected by the Holm-Bonferroni method to avoid type I error.

3. Results

3.1. Internal validation of clustering results

In this study, we applied CIMLR to investigate the heterogeneities within the MCI population. Results of the heuristic technique from CIMLR proposed in the Methods section to identify the optimal number of clusters show a dropping peak at 4 (Fig. 2.A). Therefore, four was the most optimal number of clusters for the CIMLR clustering. Table 2 shows the internal validation tests for the clustering results with the number of clusters ranging from three to ten and with the four most common clustering algorithms. Regarding the number of clusters, C=4 got the lowest Davies-Bouldin and Ray-Turi indices and the highest Silhouette and PBM indices (Table 2). In terms of the clustering results of other algorithms (K-Means, Hierarchical, PAM, CLARA), CIMLR also showed more stable results with the lowest of Davies-Bouldin and Ray-Turi and the highest Silhouette and PBM indices (Table 3). This result shows that the four clusters identified by CIMLR were the most stable result.

3.2. MCI subtypes and important features identified by cimlr

The CIMLR algorithm was applied to cluster 310 brain features extracted from sMRI of MCI patients at baseline. This analysis resulted in the identification of four distinct clusters. These clusters were visualized in a two-dimensional space, where each dimension represents a

Table 2 Clustering internal validation results using CIMLR from 03 to 10 clusters.

| Number of cluster (C) | Davies-Bouldin | Silhouette | PBM | Ray-Turi |
|-----------------------|----------------|------------|-------|----------|
| 3 | 2.724 | 0.070 | 0.838 | 2.119 |
| 4 | 2.611 | 0.071 | 1.048 | 2.001 |
| 5 | 3.055 | 0.050 | 0.718 | 2.767 |
| 6 | 3.363 | 0.038 | 0.444 | 3.438 |
| 7 | 3.418 | 0.033 | 0.432 | 3.530 |
| 8 | 3.595 | 0.024 | 0.325 | 4.682 |
| 9 | 3.534 | 0.023 | 0.323 | 5.078 |
| 10 | 3.333 | 0.019 | 0.274 | 3.945 |

Table 3Clustering internal validation results using CIMLR and four common clustering algorithms with the number of clusters is 4.

| Clustering algorithm | Davies-Bouldin | Silhouette | PBM | Ray-Turi |
|----------------------|----------------|------------|-------|----------|
| CIMLR | 2.611 | 0.071 | 1.048 | 2.001 |
| K-Means | 2.848 | 0.066 | 0.865 | 2.195 |
| Hierarchical | 2.712 | 0.067 | 1.144 | 2.135 |
| PAM | 3.937 | 0.037 | 0.827 | 6.802 |
| CLARA | 3.026 | 0.050 | 0.690 | 2.355 |

component derived through the application of t-SNE in the CIMLR algorithm (Fig. 2.B). In this visualization, each data point in each cluster is shown in the same color (Fig. 2.B). Cluster 1 contained the largest number of subjects (n=133), while cluster 3 had the smallest number of MCI patients (n=67). Cluster 2 and cluster 4 consisted of 77 and 82 subjects, respectively.

CIMLR, through learning weights for multiple kernels, enables the determination of feature ranks based on their respective kernel weights.

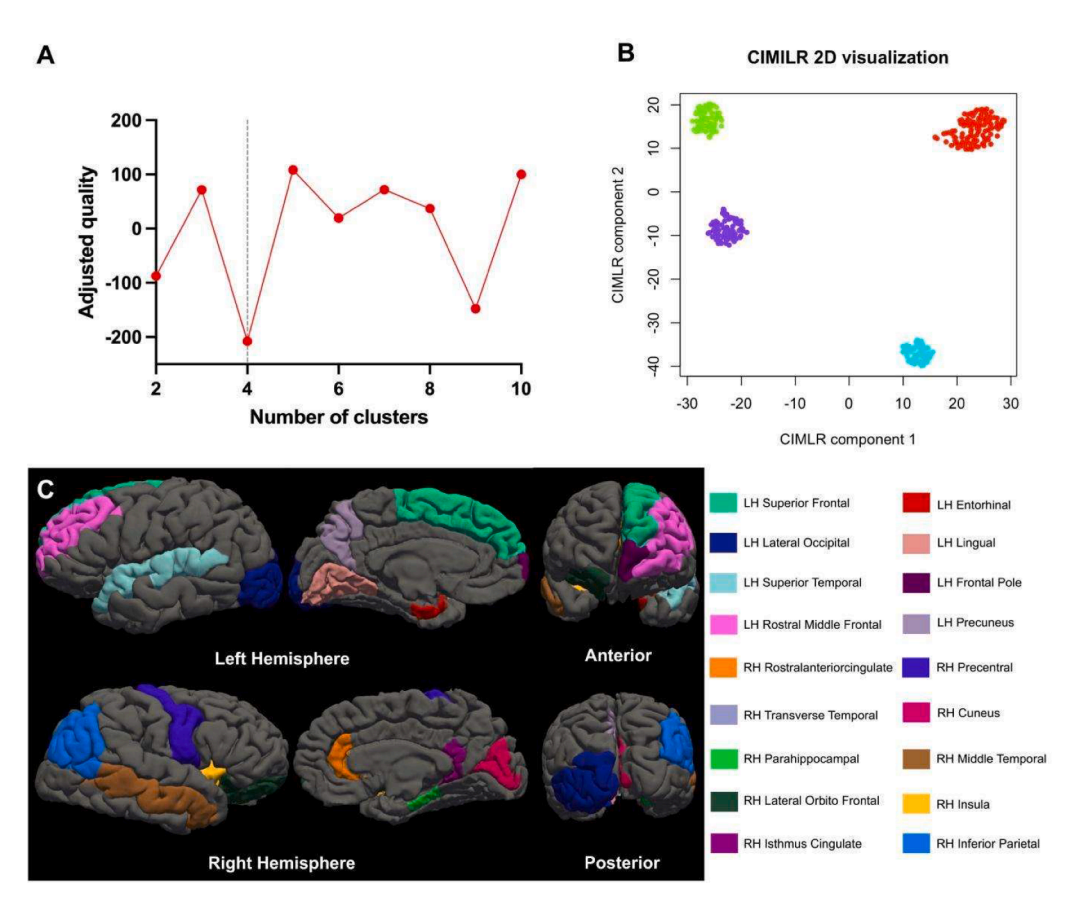


Fig. 2. Clustering results of CIMLR visualization. (A) Plot of separation cost (y-axis) suggesting 4 as the most optimal number of clusters. (B) The t-SNE 2D visualization of the 4 clusters was retrieved by CIMLR. Each cluster is identified by a color: red - cluster 1, green - cluster 2, blue - cluster 3, purple - cluster 4. (C) Labels of top 20 brain structural features. Each color in the annotation represents a distinct brain region.

In Table 4, the top 20 brain features contributing to the clustering result are presented, comprising four volume, two thickness, eight mean curvature, and six area features. The complete list of ranked features can be found in Supplement File 1. Among the top 20 features, the two most crucial ones are located in the Superior Frontal area. Other top features are located in Frontal (Right Lateral Orbitofrontal, Right Precentral), Temporal (Left Entorhinal, Right Transverse Temporal, Right Middle Temporal, Left Superior Temporal), Occipital (Left Lateral Occipital, Left Lingual), Cingulate (Right Isthmus Cingulate, Right Rostral Anterior Cingulate), and Parietal (Right Inferior Parietal) lobes, Right Parahippocampus and Right Insula Cortex. In addition, the LH Superior Frontal region ranked in the top 20 for volume and thickness, and the LH Entorhinal region appeared twice in the top 20 for volume and area. Therefore, there are only 18 regions of interest in the most important brain features ranked by CIMLR. The labels of these features are shown in Fig. 2.C.

3.3. Demographic and cognitive characteristics

We next examined the heterogeneities in the demographics and cognitive functions within the four identified MCI clusters at the baseline (Table 5). Regarding the demographic data, Cluster 2 has the highest percentage of cMCI subjects (n = 44), about 57.14%, followed by Cluster 1 (n = 65 cMCI subjects, accounting for 48.88%). The number of cMCI patients in Cluster 4 is lowest compared to the other clusters (n =31 cMCI subjects, accounting for 37.80%). Subjects in cluster 2 have the highest average age (mean age: 77.23 ± 6.95 years old), which is about five years older than participants in Cluster 4 - the youngest group (pvalue < 0.0001). For the gender distributions, the number of male subjects is more dominant in Cluster 1 and 3. There was no significant difference in years of education or distribution of APOE genotype among the four clusters. No differences were found when comparing MMSE, CDR, and FAQ scores among the four clusters. However, subjects in Cluster 2 had higher ADAS - Cog13 scores than those in Cluster 4 did (pvalue = 0.0013). In conclusion, there are significant differences in the age and gender distribution among the four clusters, but they have similar patterns in APOE4 genotype prevalence, education, and cognitive performance.

3.4. Atrophy characteristics

Fig. 3.A showed the comparison of the most important 20 features from CIMLR between each cluster and the rest of the population. Notably, five features exhibited significant differences across all

Table 4Top 20 structural brain features were retrieved by CIMLR.

| Rank | Feature Names |
|------|---|
| 1 | Left Hemisphere Superior Frontal Volume |
| 2 | Left Hemisphere Superior Frontal Thickness |
| 3 | Right Hemisphere Isthmus Cingulate Mean Curvature |
| 4 | Right Hemisphere Lateral Orbitofrontal Mean Curvature |
| 5 | Left Hemisphere Lateral Occipital Volume |
| 6 | Left Hemisphere Entorhinal Volume |
| 7 | Right Hemisphere Transverse Temporal Area |
| 8 | Right Hemisphere Precentral Mean Curvature |
| 9 | Right Hemisphere Rostral Anterior Cingulate Area |
| 10 | Left Hemisphere Superior Temporal Area |
| 11 | Left Hemisphere Precuneus Mean Curvature |
| 12 | Left Hemisphere Frontal Pole Mean Curvature |
| 13 | Left Hemisphere Entorhinal Area |
| 14 | Left Hemisphere Rostral Middle Frontal Mean Curvature |
| 15 | Right Hemisphere Inferior Parietal Area |
| 16 | Right Hemisphere Middle Temporal Area |
| 17 | Right Hemisphere Cuneus Mean Curvature |
| 18 | Right Hemisphere Parahippocampal Thickness |
| 19 | Left Hemisphere Lingual Volume |
| 20 | Right Hemisphere Insula Mean Curvature |

Table 5Comparison of demographic and cognitive characteristics among clusters.

| | Cluster 1 (<i>n</i> = 133) | Cluster 2 (<i>n</i> = 77) | Cluster 3 (<i>n</i> = 67) | Cluster 4 (<i>n</i> = 82) | p-value |
|-----------------|-----------------------------|----------------------------|----------------------------|----------------------------|--------------|
| Demographic | | | | | |
| sMCI, n | 68 | 33 | 40 | 51 | NS a |
| cMCI, n | 65 | 44 | 27 | 31 | |
| Age | 76.43 \pm | 77.23 \pm | 72.06 \pm | 72 ± 7.11 | < |
| | 6.65 | 6.95 | 7.2 | | 0.0001^{b} |
| Sex (M/F) | 116/17 | 24/53 | 56/8 | 30/52 | < |
| | | | | | 0.0001^{a} |
| Education, | $16.09\ \pm$ | 15.1 \pm | 15.62 \pm | 15.32 \pm | NS b |
| years | 2.54 | 3.33 | 3.22 | 3.33 | |
| APOE4+ (%) | 54.89 | 57.14 | 53.73 | 56.09 | NS a |
| Cognitive and m | emory | | | | |
| MMSE | 26.98 \pm | $26.58~\pm$ | 26.92 \pm | 27.32 \pm | NS b |
| | 1.75 | 1.59 | 1.84 | 1.83 | |
| CDR | 0.5 | 0.5 | 0.5 | 0.5 | NS b |
| FAQ | 4.25 \pm | 4.75 \pm | $3.49 \pm$ | 3.07 \pm | NS b |
| | 4.84 | 5.09 | 3.95 | 3.8 | |
| ADAS - Cog | 19.11 \pm | 20.64 ± 7 | 19 ± 6.62 | 16.86 \pm | 0.003 b |
| | 6.07 | | | 6.21 | |

Abbreviations: cMCI = converted Mild cognitive impairment, sMCI = stable Mild cognitive impairment, M = Male, F = Female, APOE4+ = Apolipoprotein E4 positive, MMSE = Mini-Mental State Examination, CDR = Clinical Dementia Rating, FAQ = Functional Activities Questionnaire, ADAS-Cog = Alzheimer's Disease Assessment Scale-Cognitive Subscale test, NS = Not significant. Data is illustrated as mean \pm standard deviation or number/number.

clusters, including the left Superior Frontal Thickness, left Lateral Occipital Volume, right Transverse Temporal Area, right Inferior Parietal Area, and right Middle Temporal Area (p-value < 0.05) (Fig. 3.A). However, the right Isthmus Cingulate and Insula Mean Curvatures did not show significant differences in all clusters (Fig. 3.A). The brain atrophy comparison for each cluster is depicted in Fig. 3.B, while Fig. 3.C visually represents the distinctive atrophy patterns of the four clusters, indicated by p-values obtained from the comparison between each cluster and the rest of the population.

Specifically, Cluster 3 exhibited the mildest atrophy pattern in the top 20 brain features (Fig. 3.A, Fig. 3.B). In contrast, Cluster 2 displayed the most severe atrophy compared to other cluster in nine features related to the left Superior Frontal, Temporal, left Entorhinal, right Rostral Anterior Cingulate, and left Lingual regions (Fig. 3.A, Fig. 3.B). Cluster 4 was notable for the most pronounced atrophy in the left Lateral Occipital region and decreased value of the left Precuneus, right Cuneus, right Precentral Mean Curvatures (*p-value* < 0.05) but mildest atrophy in the parahippocampal region (Fig. 3.A, Fig. 3.B). Cluster 1 generally had mild atrophy patterns similar to Cluster 3 but differed by showing significant atrophy in the right Parahippocampal region (Fig. 3.A, Fig. 3.B). The complete list of *p-values* resulting from the comparison of the top 20 brain features between each cluster and the rest of the population, and *p-values* from the Dunn's comparisons, are available in Supplementary File 2.

3.5. Plasma biomarker characteristics

At baseline, 51 biomarkers out of 191 proteins in the input data were found to be differentially expressed among the four clusters. Fig. 4 showed the comparisons of the plasma biomarker profiles of each cluster to the rest of the population and presented the results of Dunn's multiple comparisons. Cluster 1 had the greatest number of plasma markers with distinctive expression patterns (26 proteins) when compared with the rest of the population, while Cluster 3 had the lowest number of unique plasma markers (13 proteins) (Fig. 4.A). Among the markers, only Ferritin and Leptin showed significant differences in all four clusters (*p*-value < 0.01) (FSH, LH, and Testosterone were excluded due to the

^a Chi-square test.

^b Kruskal–Wallis test.

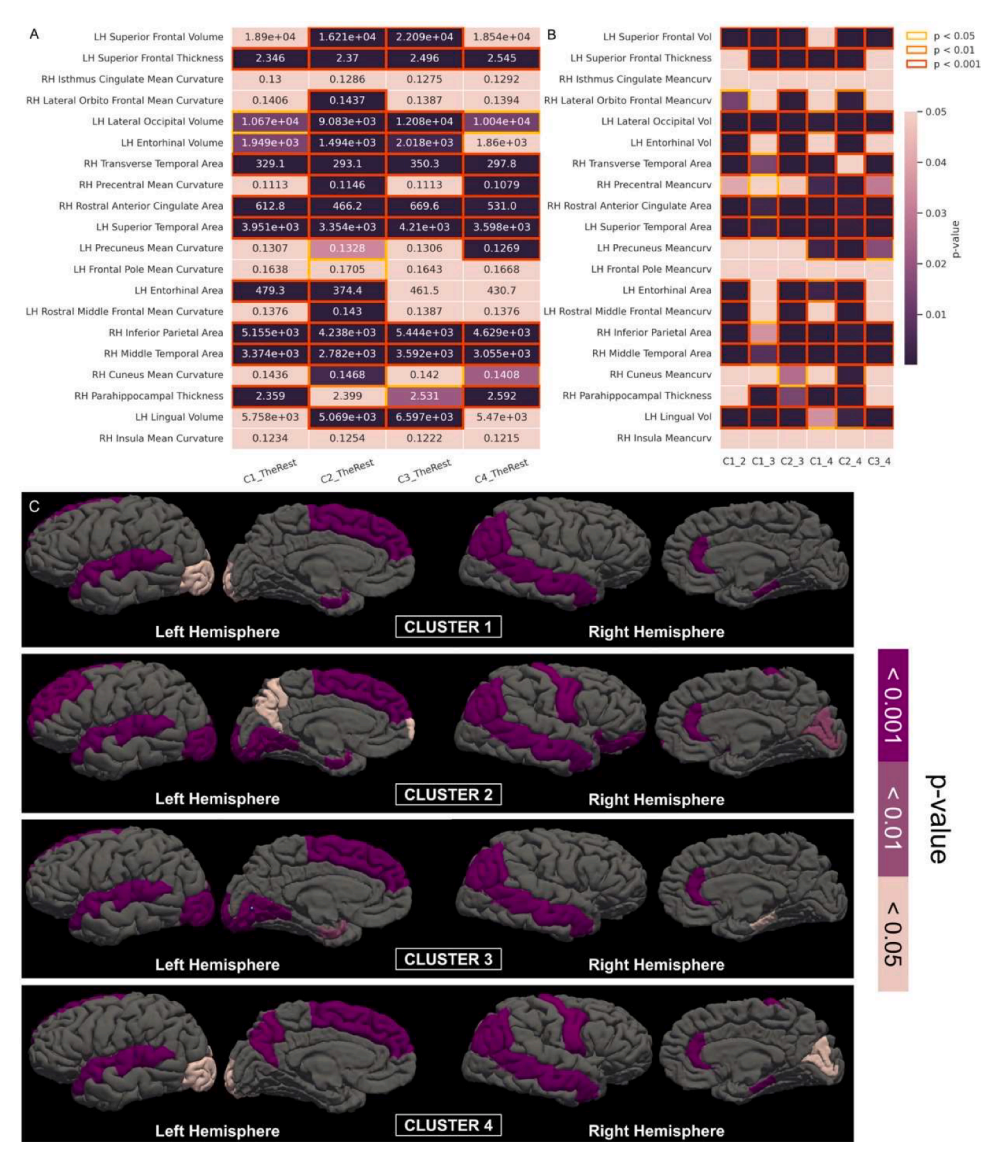


Fig. 3. (A-B) Heatmap of (A) The comparison of the top 20 brain features between each cluster and the rest of the population. (B) Dunn's comparisons of the top 20 brain features among four clusters. The colours indicate the p-values of the comparisons, and the annotation numbers indicate the mean values of each feature. (C) The atrophy patterns of each cluster. The colours represent the p-value of Fig. 3.A.

difference in gender distributions).

Cluster 1 is characterized by a significantly lower concentration of BDNF, CD40-L, GRO- α , and ENA; and a higher concentration in CgA, CK-MB, FABP, Ferritin, Creatinine, TNFR2 and Sarcosine (Fig. 4.A). Among four clusters, Cluster 2 had the highest number of statistically significant markers, with the highest values of Haptoglobin, Leptin, Adiponectin, Sortilin, and Thrombopoietin; and the lowest values of CK-MB, Calcitonin, and IL-18. More interestingly, the levels of six out of seven amino acids (His, Ile, Lys, Trp, Met, Val) in Cluster 2 were the lowest among the three. Cluster 3 and 4 shared a similar marker profile and involved the least number of AD plasma biomarkers. Nevertheless, while Cluster 3 has higher value of Calcitonin and the lowest concentration of A2Macro, BNP, MIG and TFF3; Cluster 4 presented high concentrations of Factor VII, Creatinine, and low value of TM and BLC.

In the multiple comparisons between subgroups, the total number of significantly different markers was 48 (Fig. 4.B). NFL concentration in Cluster 2 is higher than that of Cluster 3 (p-value < 0.05). Cluster 1 had a higher Cortisol concentration than Cluster 4 (p-value < 0.05) and a lower value of Leptin compared to Cluster 2 and Cluster 4 (p-value < 0.001). However, no plasma markers had significant differences in all comparisons. The complete list of p-values resulting from the comparison of

plasma biomarkers between each cluster and the rest of the population, and p-values from the Dunn's comparisons, are available in $Supplementary\ File\ 3$.

3.6. Interactions between plasma biomarkers and brain regions

Our next objective was to study the relationships between signature plasma biomarker patterns and the differences in brain atrophies of each cluster at baseline. All plasma markers having significant differences compared with the population (Fig. 4.A) were analysed for the correlation with the top 20 brain features to study the relationships between signature plasma biomarker patterns and the distinct brain atrophy characteristics of each cluster. Fig. 5 displays the significant and moderately strong correlations (p-value $<0.05,\,{\rm Rho}>0.3\,{\rm or}<-0.3)$ between plasma proteins and specific structural brain features. The complete list of the correlations, including p-value and rho value, is available in **Supplementary File 4.** Cluster 1 exhibited significant correlations between nine protein markers and seven cortical features. There were strong negative associations (p-value <0.001) between FABP, SDMA, and NFL with RH Parahippocampal Thickness; and strong positive correlations (p-value <0.001) between NGAL with LH

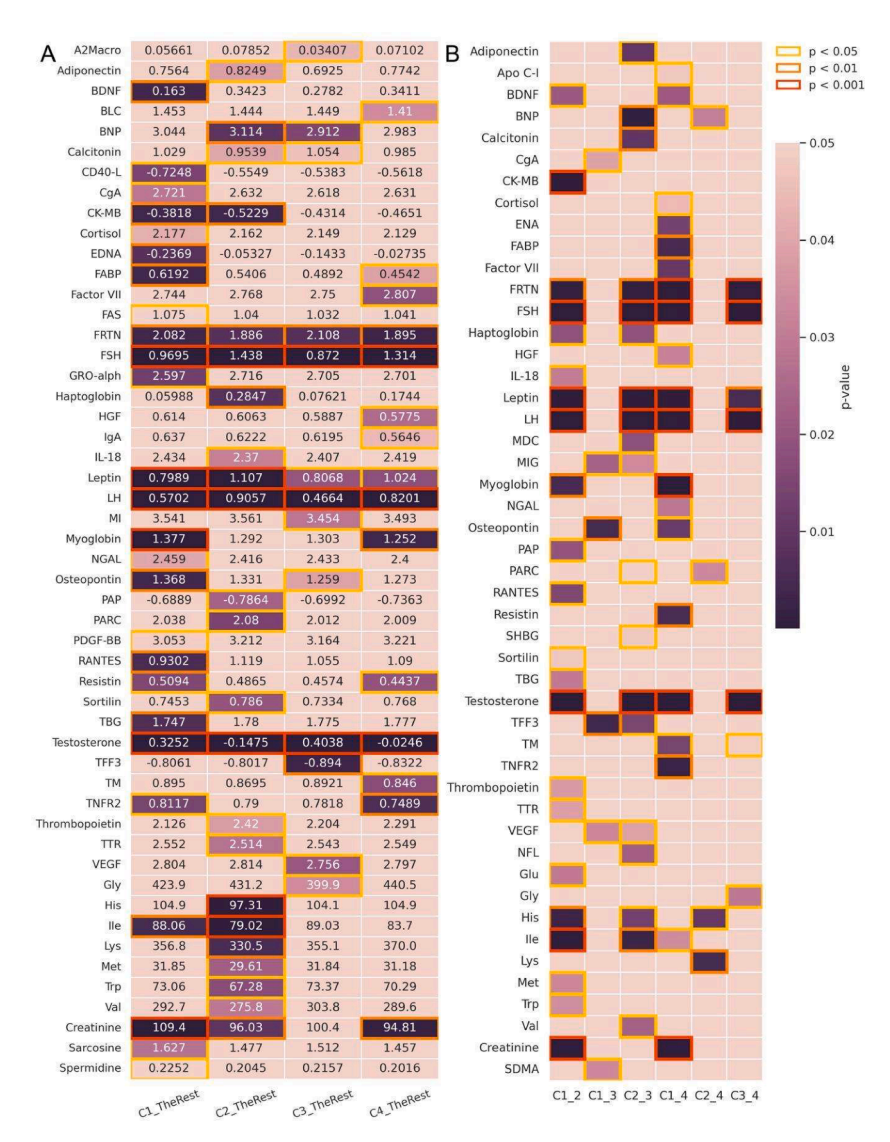


Fig. 4. Heatmap of the comparisons of plasma protein characteristics among clusters. (A) The comparison between each cluster and the rest of the population. (B) Dunn's multiple comparisons. The heatmap colours indicate the p-values of the comparisons, and the annotation numbers in Figure A indicate the mean concentrations of each protein (pre-processed by ADNI). Abbreviations: Alpha-2-Macroglobulin = A2Macro, Apolipoprotein C-I = Apo C-I Brain-Derived Neurotrophic Factor = BDNF, B Lymphocyte Chemoattractant = BLC, Brain Natriuretic Peptide = BNP, CD40 Ligand = CD40-L, Chromogranin-A = CgA, Creatine Kinase-MB = CK-MB, Epithelial-Derived Neutrophil-Activating = ENA, Fatty Acid-Binding Protein-heart = FABP, FASLG Receptor = FAS, Ferritin = FRTN, Follicle-Stimulating Hormone = FSH, Growth-Regulated alpha protein = GRO-alph, Hepatocyte Growth Factor = HGF, Immunoglobulin A = IgA, Interleukin-18 = IL-18, Luteinizing Hormone = LH, Macrophage-Derived Chemokine = MDC, Monokine Induced by Gamma Interferon = MIG, Neutrophil Gelatinase-Associated Lipocal = NGAL, Prostatic Acid Phosphatase = PAP, Pulmonary and Activation-Regulated Chemo = PARC, Platelet-Derived Growth Factor BB = PDGF-BB, Sex Hormone-Binding Globulin = SHBG, T-Cell-Specific Protein RANTES = RANTES, Thyroxine-Binding Globulin = TBG, Trefoil Factor 3 = TFF3, TM = Thrombomodulin, Tumor Necrosis Factor Receptor-Like 2 = TNFR2, Transthyretin = TTR, Vascular Endothelial Growth Factor = VEGF, Symmetric dimethylarginine = SDMA.

Precuneus Meancurv and Apo-C1 with LH Rostral Middle Frontal Meancurv. On the other hand, in Cluster 2, Apo-C1 showed a negative correlation with LH Rostral Middle Frontal Meancurv. Moreover, the RH Parahippocampal Thickness in Cluster 2 showed positive correlations with six amino acid markers (Trp, Ile, Val, Glu, His, Met). Cluster 3 had seven proteins significantly correlated (p-value <0.001) with the brain features, four of which displayed a positive correlation, while the others showed an inverse relationship with the markers. In Cluster 4, seven out of eight protein markers presented negative correlations with RH Precentral Meancurv (p-value <0.05), with the most significant proteins being FABP and NGAL (p-value <0.001) (Fig. 5).

3.7. Longitudinal analyses of cognitive characteristics

To assess the rate of disease progression, a longitudinal evaluation

from baseline to 36-month follow-up was conducted based on cognitive and neuropsychological performance, by using four tests: MMSE, CDR, FAQ, and ADAS- Cog-13 (Fig. 6.A). Table 6 displays the Slope values of the linear regressions from Fig. 6.A. Cluster 2 showed the highest rate of cognitive decline, shown by the peak slope values in all tests, followed by Cluster 1, with the second highest values in the MMSE, CDR, and FAQ scores. Clusters 3 and 4 both showed a mild cognitive decline with similar slopes across four tests, but cluster 4 displayed a slightly milder decline.

Longitudinal correlations between the four cognitive test results and the plasma proteins were analyzed over 36 months and shown in Fig. 6. B. Only significant correlations were reported. There were five protein markers that could possibly be indicative of the cognitive decline rate in MCI patients. Specifically, higher concentrations of plasma NFL and Cortisol, in particular, may be linked with a faster cognitive decline rate.

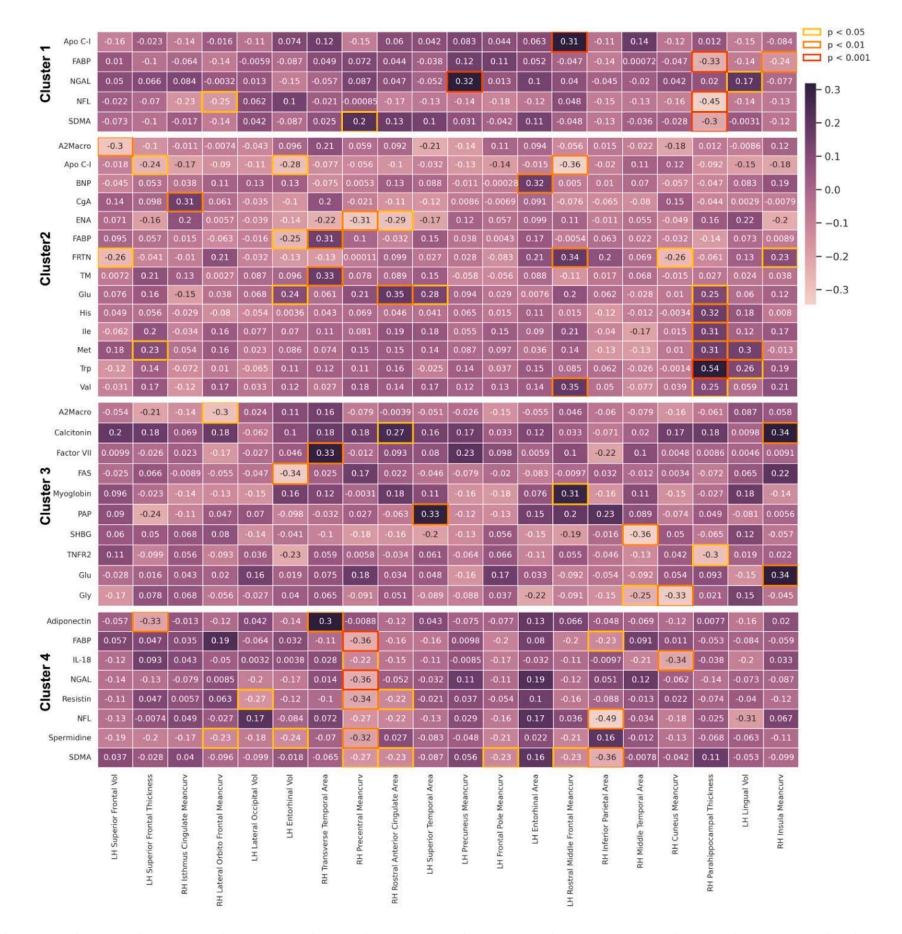


Fig. 5. Heatmap depicting the correlations between the top 20 brain features and unique plasma protein biomarkers of each cluster. The heatmap colours and the annotation numbers depict the Rho values. The color of the square borders indicates the p-value of the correlation between each marker and brain region.

In contrast, patients with higher Hepatocyte Growth Factor (HGF), B Lymphocyte Chemoattractant (BLC), and Interleukin-18 (IL-18) were likely to have slower decreases in cognitive functions (Fig. 6.B).

3.8. Longitudinal analyses of brain atrophy characteristics

Longitudinal changes in brain atrophy were investigated by tracking the top 20 brain features in three years, and only statistically significant results (p-value < 0.05) were chosen to be represented in Fig. 7.A. Then, features with significant changes were further examined for correlations with cognitive test result changes (Fig. 7.B). Table 7 shows the Slopes of the linear regression analyses in four clusters in three-year-time. There were six features showing consistent decreasing trends in all four clusters (Fig. 7.A and Table 6). Amongst the other features, LH Lateral Occipital and Superior Frontal volumes showed the steepest degeneration in Cluster 3 (Lateral Occipital - slope = -18.5 and Superior Frontal - slope = -35.5).

Cluster 3 had the most rapid atrophy pattern, with significantly decreasing trends in five out of seven cortical features and the highest negative slope in the LH Superior Frontal, LH Lateral Occipital area, and LH Entorhinal Volume. Cluster 2 decreasing trends were only significant in the LH Entorhinal Volume, however, the LH Superior Frontal Thickness showed the second highest negative slope compared to the other clusters. On the other hand, the cognitive trajectory in the MCI population is mostly inversely correlated with nine brain features (Fig. 7.B). Amongst them, LH Lateral Occipital Volume, LH Entorhinal Volume, RH Parahippocampal Thickness, and RH Inferior Parietal Area showed the most significant correlation with cognitive function test scores and hence could be indicative of cognitive decline.

4. Discussion

In this study, we employed the CIMLR clustering algorithm to investigate the heterogeneity of the MCI population using structural MRI from the ADNI database. We used FreeSurfer to extract a total of 310 morphometric features from T1-weighted MRI (including 106 vol, 68 area, 68 thickness, and 68 mean curvature features) of 359 MCI subjects. Then, the CIMLR clustered patients into four subgroups and also ranked these 310 features based on their contribution to the clustering process. Four clusters were then examined for their differences in cognitive scores, top 20 important brain features, proteomic profiles, and their corresponding longitudinal correlations at baseline and 36 months follow-up. The heterogeneities in atrophy patterns and biological processes of these four clusters were examined through the differences in morphometric sMRI features and plasma proteins. At the baseline, all subgroups presented non-significant differences in education levels, APOE4 prevalence, and cognitive scores, including MMSE, CDR, FAQ, and ADAS-CoG (Table 5). Despite this initial similarity, we identified four distinct brain atrophy patterns based on the MRI features, which correspond to different plasma biomarkers and cognitive degeneration rates for both cross-sectional and longitudinal data (Table 8).

In general, Clusters 1 and 2 displayed the highest number of converter MCI with an older average age above 76 compared to Cluster 3 and 4. More specifically, Cluster 2 stood out with the highest AD risk due to the most severity of brain atrophy at baseline, as evidenced by severe cortical shrinkages in the AD-related regions, including the temporal, entorhinal, rostral anterior cingulate, and lingual regions (Fig. 3) [32, 33], and the fastest cognitive decline (Fig. 6.A). Cluster 1, despite having the second to highest average age, had moderate brain shrinkage and a similar atrophy pattern to Cluster 3 (Fig. 3). To delineate the

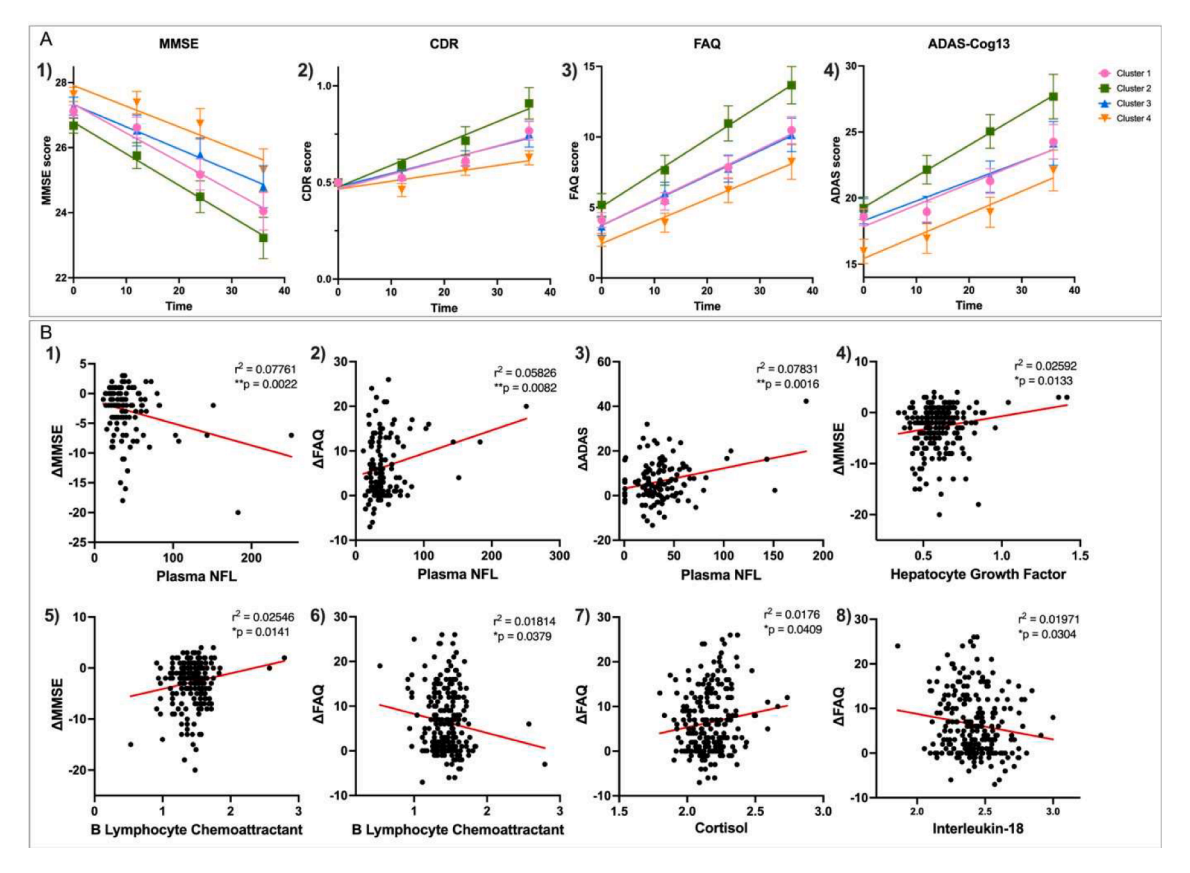


Fig. 6. The longitudinal analyses over 36 months of cognitive performance among four clusters. (A) Linear regression graphs indicated the longitudinal analysis of cognitive characteristics from the Baseline stage to month 36th among clusters. (B) The linear relationships between the changes of cognitive tests and plasma proteins.

Table 6Linear regression slopes of four cognitive tests from baseline to 36 months.

| Cognitive test | Cluster 1 | Cluster 2 | Cluster 3 | Cluster 4 |
|--------------------|--|---|---|--|
| MMSE CDR FAQ | - 0.08876*** 0.007413*** 0.1795*** | - 0.09677*** 0.01127*** 0.2396*** | - 0.06812** 0.006979*** 0.1766*** | - 0.06362** 0.004085** 0.1573*** |
| ADAS-Cog13 | 0.1622*** | 0.2353*** | 0.1493* | 0.1697** |

Abbreviations: MMSE = Mini-Mental State Examination, CDR = Clinical Dementia Rating, FAQ = Functional Activities Questionnaire, ADAS-Cog = Alzheimer's Disease Assessment Scale-Cognitive Subscale test.

heterogeneous properties between the clusters, we then analyzed the atrophy pattern and plasma protein expression within each group.

4.1. Exploring heterogeneity by multi-faceted analysis of brain features

Although numerous studies on MCI heterogeneity have focused on analyzing volume-based or gray matter features from neuroimaging data, emerging evidence has suggested that other morphometrics such as curvature, area, or thickness of the cortical regions and subregions could provide benefits over measuring volumes [34–36]. In this study, we combined multiple types of structural MRI features extracted from FreeSurfer, including volume, thickness, area, and curvature of different brain regions to cluster the MCI population. This strategy allows us to employ a multi-faceted analysis of atrophy, as each type of feature provides a distinct perspective on assessing the extent of atrophy. For instance, previous research suggests that mean curvature features can

indicate white matter atrophy, with higher mean curvature values in a brain region corresponding to greater severity of white matter damage [37,38]. By incorporating these diverse features, we can gain a more nuanced understanding of the atrophy patterns within the MCI population.

4.2. Brain atrophy patterns of high-risk clusters

Using the features from FreeSurfer, our analysis revealed four distinct MRI-based regional atrophy patterns (Fig. 3). The top 20 MRI-derived features identified by CIMLR in our study reflected the brain regions that were previously reported to correlate with AD progression [39–42]. Moreover, the heterogeneities in these top 20 features (Table 4) were also documented in precedent research [15,17,43,44].

In more detail, Cluster 2 showed the most severe atrophy with a diffuse pattern and severe brain atrophy in the temporal, frontal lobes, and the entorhinal cortex. This pattern closely mirrors the progression of tau pathology as described in the Braak staging system. According to this system, the initial stages of atrophy are observed in the entorhinal region and midbrain areas, from where it progressively extends to the frontal and temporal lobes, impacting the parietal and occipital lobes [45,46]. These atrophy were the most severe in four cortical areas that overlap with typical AD cluster in other heterogeneity research [47–49], including Frontal, Precuneus, Temporal, Lateral Occipital regions, and Entorhinal cortex. For instance, the Li study's atrophy map of AD patients identified major brain atrophy in the temporoparietal, cingulate gyrus, precuneus, and occipital regions, while its frontal variant involved cortical shrinkage in the frontal cortical areas.

On the other hand, compared to the Whitwell study, the atrophy pattern of Cluster 2 was a mix between the typical AD group and the limbic-predominant group, where affected areas included the temporal,

^{*} p-value <0.05.

^{**} p-value <0.01.

^{***} p-value <0.001.

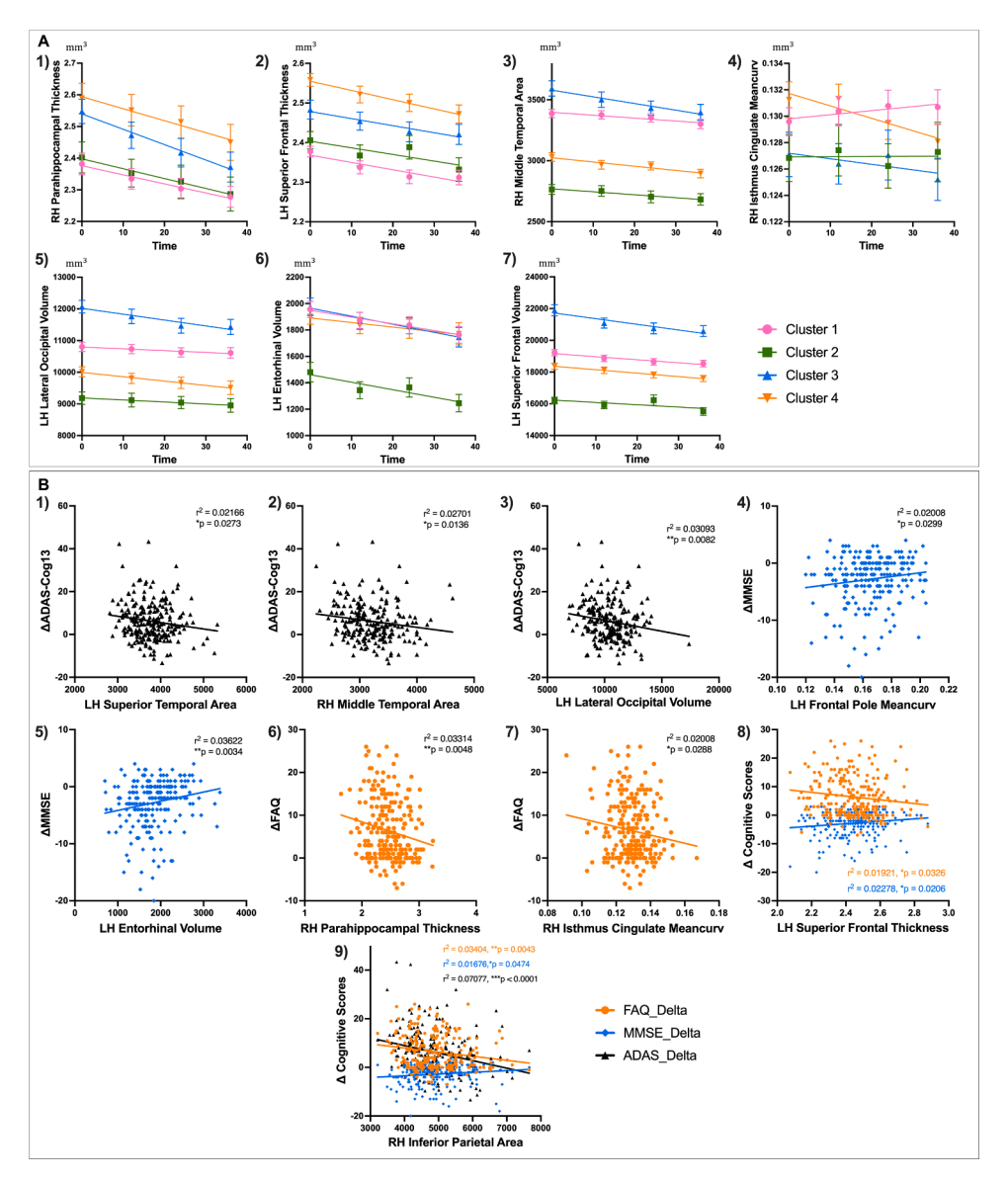


Fig. 7. The longitudinal analyses over 36 months of the statistically significant brain features selected from the top 20 among four clusters. (A) Linear regression graphs indicated the longitudinal analysis of brain feature changes from baseline to month 36th. (B) The linear relationships between the changes of cognitive tests and brain atrophy.

Table 7Linear regression slopes of brain atrophy with significant change in 3-year-time.

| Features | Cluster 1 | Cluster 2 | Cluster 3 | Cluster 4 |
|-------------------------------|-----------------------|------------------------|-------------------------|-------------------------|
| RH Middle Temporal Area | -2.377 | -2.44 | −5.469 * | -3.457** |
| RH Isthmus Cingulate Meancurv | $3.083 	imes 10^{-5}$ | 1.344×10^{-6} | -4.189×10^{-5} | $-9.425 	imes 10^{-5*}$ |
| LH Superior Frontal Thickness | -0.00184** | -0.00167 | -0.001784 | -0.002328** |
| RH Parahippocampal Thickness | -0.002861* | -0.003112 | -0.004851** | -0.003785* |
| LH Entorhinal Volume | -5.096* | -5.698* | -6.097 * | -3.466 |
| LH Lateral Occipital Volume | -5.685 | -6.39 | -18.5* | -13.73* |
| LH Superior Frontal Volume | -19.07* | -14.53 | -35.55** | -21.64** |

Abbreviations: LH: Left hemisphere, RH: Right hemisphere.

frontal lobes, and the entorhinal cortex [46]. From the discussed examples, our results suggested the pattern of atrophy in Cluster 2 could be indicative of typical AD progression, which is strengthened by its worst cognitive decline after 36 months and well-aligned with previous studies.

Cluster 4 presented an anatomical atrophy similar to Cluster 2 but with lesser degeneration, but this cluster has the best thickness of the right Parahippocampus. During AD development and progression, the Hippocampal and its related structures such as the Parahippocampal regions are the earliest and most severely affected brain regions. In

^{*} p-value <0.05.

^{**} p-value <0.01

^{***} p-value <0.001.

Table 8Summary of the heterogeneity of four proposed MCI clusters.

| | Cluster 1 | Cluster 2 | Cluster 3 | Cluster 4 |
|----------------------|---|---|--------------------|--|
| Demographics | Old age group | Old age group | Young age group | Young age group |
| Cognitive decline | Slow | Fastest | Slow | Slowest |
| Brain atrophy | Mild atrophy More temporal and occipital dominant atrophy | Most severe atrophy in AD-related regions, including the temporal, entorhinal, rostral anterior cingulate, and lingual regions | Mildest atrophy | Quite severe atrophy Similar pattern to C2 Parahippocampus: thickest |
| Plasma biomarkers | High TNFR2- Low BDNF and CD40L | High Leptin, Adiponectin, and CKMB Positive correlation: amino acids and Parahippocampal atrophy Low tryptophan | Low MIG | Low Thrombomodulin and B Lymphocyte Chemoattractant |

contrast, most cortical shrinkages in Cluster 4 were in the Occipital and the Precuneus regions, which are not normally observed in AD atrophy patterns but in Posterior Cortical Atrophy, a less common form of dementia. Therefore, these results implied a lower incident risk for AD in Cluster 4 as this cluster did not exhibit atrophy in AD-related brain regions, and suggested mixed dementia, where cognitive decline is concurrently caused by other types of dementia, such as Posterior Cortical Atrophy.

Compared to them, Cluster 1 and 3 had the mildest brain atrophy with similar morphometric values in 10 out of the top 20 brain features, specifically the superior frontal, superior temporal, lingual, and occipital regions. Despite sharing great atrophy similarity, the cortical damage in the Lingual and Temporal areas of Cluster 3 was significantly less severe than in Cluster 1, suggesting a more temporal and occipitaldominant atrophy in Cluster 1 compared to Cluster 3. On the other hand, compared to the Ten Kate study, Cluster 3 and 1 displayed a different class exhibiting predominant medial-temporal and parietooccipital atrophy [4]. On the other hand, longitudinal analysis showed a negative correlation between the Left Lateral volume, Entorhinal volume, RH Parahippocampal thickness, Inferior Parietal area, and the cognitive decline trajectory of all four MCI subtypes, reflecting on the worsening cognitive scores. These findings align with a previous study, which found that the decrease in volume of the temporal and parietal lobes correlated with the severity of cognitive impairment and the development of neurodegeneration [41,50,51].

In brief, our study identified four different atrophy patterns based on sMRI morphometric features obtained from FreeSurfer with Cluster 4 resembling typical AD atrophy, Cluster 2 as non-AD mix atrophy, and Cluster 1 and 3 as the mildest MCI subgroups. Based on these results, we further addressed the anatomical variation of cortical degeneration in MCI patients, particularly for subgroups with equivalent levels of brain atrophy and similar demographic profiles at baseline.

4.3. Cardiovascular and metabolic mechanisms contributing to AD progression

After clustering the MCI populations into four groups with heterogeneous atrophy profiles, we examined the variation in plasma marker expression. Among the four subgroups, Cluster 2 has the most significant number of AD-related indicators, which were inversely correlated with cognitive outcomes. These biomarkers are involved in various degeneration pathways, including cardiovascular diseases (CVDs), amino acids deficit, and lipid metabolisms. Abnormally elevated levels of Leptin, Adiponectin, and CKMB indicate the presence of CVDs and cardiac diseases that can traverse to the nervous system damaging the neuronal networks and synapses [52-54]. Moreover, we observed a positive relationship between the amino acids level and the Parahippocampal atrophy in Cluster 2, consistent with previous studies linking amino acid metabolism to AD and cognitive trajectory [55,56]. Notably, tryptophan and its intermediate metabolites can modulate AD development by regulating neuro-inflammation, amyloid-beta synthesis, as well as causing sleep disorders that affect amyloid-beta clearance [57,58]. Abnormal levels of these markers suggested a multi-factor mechanism contributing to AD development in Cluster 2, explaining the cluster's poorest cognitive scores and severe atrophy.

4.4. Protective biological markers mitigate AD progression

Compared to Cluster 2, despite having a similar average age, Cluster 1 showed a lower incidence of cMCI and less severe brain atrophy compared to Cluster 2, indicating that age alone does not determine the severity of disease progression. This variation may be attributed to the presence of protective biological markers, such as TNFR2, which acts as an immune modulator with strong anti-inflammatory effects, and therefore causes protective effects on the oligodendrocytes and neurons, promoting cell survival [59,60]. Cluster 1 also displayed low levels of BDNF and CD40 Ligand, which are involved in inflammation pathways as indicators and modulators [61,62]. These markers may protect Cluster 1 from inflammatory damage, which is considered a major mechanism leading to AD. Conversely, Cluster 1 showed high levels of FABP and Ferritin. While Ferritin is known for the storage of iron ions, FABP is a lipid-binding protein that facilitates the intracellular transportation of fatty acids into the nerve cells, which might pose a risk for AD development [63,64]. However, the negative impact of these factors seems to be mitigated by the anti-inflammatory markers, resulting in a slower progression of degeneration within Cluster 1 due to a balance between harmful and protective mechanisms, particularly involving iron deposition and lipid metabolism abnormalities in the central nervous system (CNS).

Clusters 3 and 4 displayed a similar marker profile, particularly with the lowest level of MIG (CXCL9). It's important to note that Cluster 3 displayed the mildest atrophy at baseline and a mild cognitive decline over time. This align with previous study, MIG, particularly circulating MIG, level was high in AD patients and suggestively associated with a higher risk of AD [65–67]. This may be related to MIG is present in the Central Nervous System and is related to pro-inflammation and endothelial dysfunction [68].

4.5. Potential plasma biomarkers for early diagnosis

Longitudinal analyses of cognitive performance revealed increased levels of Cortisol and NFL may link with a faster cognitive decline; and higher levels of Hepatocyte Growth Factor (HGF), B lymphocyte chemoattractant (BLC), and interleukin-18 (IL-18) correlate with slower decreases in cognitive functions. This is consistent with previous research that a long-term increase of Cortisol and NFL was associated with a faster progression of AD, and suggested the role of these two proteins as potential preclinical markers for AD [69–72]. On the other hand, higher levels of HGF in CSF at baseline can be indicative of a faster cognitive decline in both MCI and AD patients and associated with Small vessel disease dementia [73,74]. However, the HGF/c-Met-receptor system activation is reported to be associated with various biological processes including mitogenesis, motogenesis, morphogenesis, stem cell differentiation, and neurogenesis. These processes have the potential to

prevent neuroinflammation, oxidative stress-induced damage, neurotoxicity, which can halt the progression of AD [75,76]. Interestingly, another study demonstrated that the expression of IL-18, which is associated with neuroinflammatory processes, reaches its peak during the MCI stage and decreases during the AD stage, aligning with the findings of our study [77]. However, there is limited evidence supporting the role of BLC in AD pathology. In conclusion, HGF was further confirmed as a potential treatment strategy for AD and dementia, while Cortisol and NFL were identified as potential prognostic biomarkers for assessing the severity of cognitive decline. Further investigation is needed to understand the patterns of IL-18 expression in MCI converted to AD.

4.6. Limitations and future directions

Our study had several limitations owing to its limited sample size and longitudinal data availability. Firstly, the sample size in the study was limited as we aimed to characterize both MRI-based brain atrophy and plasma protein profile, so only subjects with both information accessible were included. Secondly, there were cases of missing data, particularly follow-up sMRI after 36 months, because of the high drop-off and mortality rate as the disease progressed in high-risk patients. Consequently, those limitations may lead to large standard deviations and insignificance in statistical analysis. Thirdly, because of the complexity of the study design and the impracticality of thoroughly analyzing all 310 features, this study only focused on the top 20 brain features, which did not include the medial temporal region - an important region for AD. Therefore, the future analysis could expand our study scope and include more brain regions in the CIMLR clustering step, and increase the sample size both regionally and globally to study the MCI heterogeneity more comprehensively. Although there had been numerous research developing blood tests and exploring potential markers for the diagnosis of AD, yet, the efficacy of these blood markers varied across studies within the same population and ethnic community [78-80]. One possible confounding factor that causes these variations is the disease heterogeneity and even its precedent stage - MCI. The findings and pipeline we proposed in this study can be employed for similar studies on other datasets or larger populations to find the characteristic biomarker panels that can be used for early AD screening and diagnosis. Therefore, taking into account this heterogeneity of the MCI stage in biomarkers exploration study could resolve the current limitation and inconsistency of previous research, and further enhance AD early diagnosis and prognosis accuracy.

5. Conclusion

This study identified four different clusters in the MCI population by the data-driven clustering approach based on imaging data. Although four clusters had the same cognitive performance with the traditional diagnostic methods at the baseline, these clusters displayed distinct brain atrophy, plasma biomarkers, and cognitive progression characteristics. Parahippocampal atrophy was found to be positively correlated with cognitive impairment and amino acid levels. The study also identified several factors that can alleviate or worsen the progression of the MCI including lipid and amino acid metabolism, cardiovascular diseases, inflammatory modulators, and glial activations. These findings suggest that the current clinical practice is not sensitive to detect the early changes of AD. The longitudinal analyses showed the potential of HGF as a slow cognitive impairment marker; Cortisol and NFL as prognosis markers for aggressive MCI progression. These findings provide valuable insights for future research, contributing to the accurate diagnosis and precision medicine for MCI progression and AD.

Statement of significance

Current treatments fail to halt the progression of Alzheimer's disease

(AD) due to the clinical, pathological, and morphological heterogeneities of the AD spectrum. Emerging evidence has suggested that these heterogeneous characteristics can be rooted back to the early stages of AD - mild cognitive impairment (MCI). Addressing these heterogeneities at the MCI stage when the disease has not reached an irreversible status can allow the development of early and timely interventions to manage AD more effectively. Therefore, in this study, we aim to investigate the heterogeneity of the MCI population based on structural brain imaging using clustering methods. This method will cluster the MCI population into subgroups, which are called clusters. The heterogeneous characteristics of each cluster were then analyzed in terms of cognitive trajectories, brain atrophy, and plasma biomarkers at the baseline and after longitudinal changes. We identified four clusters with distinct progression rates and proteomic profiles using the CIMLR algorithm, suggesting potential markers and approaches for personalized AD diagnosis and management.

Ethical Statement

The data used in the manuscript: "Revealing the heterogeneity of plasma protein and cognitive decline trajectory among Mild Cognitive Impairment patients by clustering of brain atrophy features" was from Alzheimer's Disease Neuroimaging Initiative (ADNI) database.

ADNI obtained all IRB approvals and met all ethical standards in the collection of data. The following are the ethics committees and IRB boards that provided approval. The Ethics committees/institutional review boards that approved the ADNI study are: Albany Medical Center Committee on Research Involving Human Subjects Institutional Review Board, Boston University Medical Campus and Boston Medical Center Institutional Review Board, Butler Hospital Institutional Review Board, Cleveland Clinic Institutional Review Board, Columbia University Medical Center Institutional Review Board, Duke University Health System Institutional Review Board, Emory Institutional Review Board, Georgetown University Institutional Review Board, Health Sciences Institutional Review Board, Houston Methodist Institutional Review Board, Howard University Office of Regulatory Research Compliance, Icahn School of Medicine at Mount Sinai Program for the Protection of Human Subjects, Indiana University Institutional Review Board, Institutional Review Board of Baylor College of Medicine, Jewish General Hospital Research Ethics Board, Johns Hopkins Medicine Institutional Review Board, Lifespan - Rhode Island Hospital Institutional Review Board, Mayo Clinic Institutional Review Board, Mount Sinai Medical Center Institutional Review Board, Nathan Kline Institute for Psychiatric Research & Rockland Psychiatric Center Institutional Review Board, New York University Langone Medical Center School of Medicine Institutional Review Board, Northwestern University Institutional Review Board, Oregon Health and Science University Institutional Review Board, Partners Human Research Committee Research Ethics, Board Sunnybrook Health Sciences centre, Roper St. Francis Healthcare Institutional Review Board, Rush University Medical Center Institutional Review Board, St. Joseph's Phoenix Institutional Review Board, Stanford Institutional Review Board, The Ohio State University Institutional Review Board, University Hospitals Cleveland Medical Center Institutional Review Board, University of Alabama Office of the IRB, University of British Columbia Research Ethics Board, University of California Davis Institutional Review Board Administration, University of California Los Angeles Office of the Human Research Protection Program, University of California San Diego Human Research Protections Program, University of California San Francisco Human Research Protection Program, University of Iowa Institutional Review Board, University of Kansas Medical Center Human Subjects Committee, University of Kentucky Medical Institutional Review Board, University of Michigan Medical School Institutional Review Board, University of Pennsylvania Institutional Review Board, University of Pittsburgh Institutional Review Board, University of Rochester Research Subjects Review Board, University of South Florida Institutional Review Board, University of

Southern, California Institutional Review Board, UT Southwestern Institution Review Board, VA Long Beach Healthcare System Institutional Review Board, Vanderbilt University Medical Center Institutional Review Board, Wake Forest School of Medicine Institutional Review Board, Washington University School of Medicine Institutional Review Board, Western Institutional Review Board, Western University Health Sciences Research Ethics Board, and Yale University Institutional Review Board.

All necessary patient/participant consent has been obtained and the appropriate institutional forms have been archived. For more information, please visit: https://adni.loni.usc.edu/wp-content/uploads/2017/09/ADNID Approved Protocol 11.19.14.pdf

CRediT authorship contribution statement

My Nguyen: Conceptualization, Data curation, Formal analysis, Investigation, Methodology, Project administration, Software, Validation, Visualization, Writing – original draft, Writing – review & editing. Bao Pham: Formal analysis, Writing – original draft, Writing – review & editing. Toi Vo: Funding acquisition. Huong Ha: Conceptualization, Funding acquisition, Investigation, Supervision, Validation, Writing – review & editing.

Declaration of competing interest

The authors declare that they have no known competing financial interests or personal relationships that could have appeared to influence the work reported in this paper.

Data availability

The authors do not have permission to share data.

Acknowledgements

Data used in preparation of this article were obtained from the Alzheimer's Disease Neuroimaging Initiative (ADNI) database (adni.loni. usc.edu) and the Alzheimer's Disease Metabolomics Consortium (ADMC). As such, the investigators within the ADNI contributed to the design and implementation of ADNI and/or provided data but did not participate in analysis or writing of this report. A complete listing of ADNI investigators can be found at: http://adni.loni.usc.edu/wpcontent/uploads/how_to_apply/ADNI_Acknowledgement_List.pdf and https://sites.duke.edu/adnimetab/team

My Nguyen is funded by ADAI-Lab under the "ADAI Fellowship" program. Huong Ha and Toi Vo are funded by Vietnam National University Ho Chi Minh City (VNU-HCM) under grant number NCM2020–28–01.

Supplementary materials

Supplementary material associated with this article can be found, in the online version, at doi:10.1016/j.brain.2024.100093.

References

- R.A. Armstrong, L. Wood, The identification of pathological subtypes of Alzheimer's disease using cluster analysis, Acta Neuropathol. 88 (1) (1994) 60–66.
- [2] Y. Noh, et al., Anatomical heterogeneity of Alzheimer disease: based on cortical thickness on MRIs, Neurology. 83 (21) (2014) 1936–1944.
- [3] B. Lam, et al., Clinical, imaging, and pathological heterogeneity of the Alzheimer's disease syndrome, Alzheimers. Res. Ther. 5 (1) (2013) 1–14.
- [4] M. Ten Kate, et al., Atrophy subtypes in prodromal Alzheimer's disease are associated with cognitive decline, Brain 141 (12) (2018) 3443–3456.
- [5] D. Ferreira, L.O. Wahlund, E. Westman, The heterogeneity within Alzheimer's disease, Aging (Albany. NY) 10 (11) (2018) 3058.

- [6] S.R Das, et al., Tau-Atrophy Variability Reveals Phenotypic Heterogeneity in Alzheimer's Disease, Ann. Neurol. 90 (5) (2021) 751–762.
- [7] P. Chen, et al., Four distinct subtypes of Alzheimer's disease based on resting-state connectivity biomarkers, Biol. Psychiatry (2022).
- [8] M.E. Murray, et al., Neuropathologically defined subtypes of Alzheimer's disease with distinct clinical characteristics: a retrospective study, Lancet Neurol. 10 (9) (2011) 785–796.
- [9] K. Poulakis, et al., Heterogeneous patterns of brain atrophy in Alzheimer's disease, Neurobiol. Aging 65 (2018) 98–108.
- [10] J. Escudero, J.P. Zajicek, E. Ifeachor, Early detection and characterization of Alzheimer's disease in clinical scenarios using Bioprofile concepts and K-means, in: 2011 Annual International Conference of the IEEE Engineering in Medicine and Biology Society, IEEE, 2011.
- [11] M. Kärkkäinen, et al., Structural brain imaging phenotypes of mild cognitive impairment (MCI) and Alzheimer's disease (AD) found by hierarchical clustering, International Journal of Alzheimer's Disease (2020), 2020.
- [12] A. Mitelpunkt, et al., Novel Alzheimer's disease subtypes identified using a data and knowledge driven strategy, Sci. Rep. 10 (1) (2020) 1–13.
- [13] N. Toschi, et al., Biomarker-guided clustering of Alzheimer's disease clinical syndromes, Neurobiol. Aging 83 (2019) 42–53.
- [14] S.L. Risacher, et al., Alzheimer disease brain atrophy subtypes are associated with cognition and rate of decline, Neurology. 89 (21) (2017) 2176–2186.
- [15] G. Martí-Juan, et al., Revealing heterogeneity of brain imaging phenotypes in Alzheimer's disease based on unsupervised clustering of blood marker profiles, PLoS. One 14 (3) (2019) e0211121.
- [16] C. Wu, et al., Discrimination and conversion prediction of mild cognitive impairment using convolutional neural networks, Quant. ImAging Med. Surg. 8 (10) (2018) 992.
- [17] J. Nettiksimmons, et al., Biological heterogeneity in ADNI amnestic mild cognitive impairment, Alzheimer's & Dementia, 10 (5) (2014) 511–521, e1.
- [18] X. Ding, et al., A hybrid computational approach for efficient Alzheimer's disease classification based on heterogeneous data, Sci. Rep. 8 (1) (2018) 1–10.
- [19] D. Gamberger, et al., Identification of clusters of rapid and slow decliners among subjects at risk for Alzheimer's disease, Sci. Rep. 7 (1) (2017) 1–12.
- [20] E. McDade, et al., Longitudinal cognitive and biomarker changes in dominantly inherited Alzheimer disease, Neurology. 91 (14) (2018) e1295–e1306.
- [21] D. Goyal, et al., Characterizing heterogeneity in the progression of Alzheimer's disease using longitudinal clinical and neuroimaging biomarkers, Alzheimer's & Dementia: Diagnosis, Assessment & Disease Monitoring 10 (2018) 629–637.
- [22] D. Ramazzotti, et al., Multi-omic tumor data reveal diversity of molecular mechanisms that correlate with survival, Nat. Commun. 9 (1) (2018) 1–14.
- [23] B. Fischl, FreeSurfer, Neuroimage 62 (2) (2012) 774-781.
- [24] H. Ong, et al., A Machine Learning Framework Based on Extreme Gradient Boosting for Intelligent Alzheimer's Disease Diagnosis Using Structure MRI, in: International Conference on the Development of Biomedical Engineering in Vietnam, Springer, 2020.
- [25] B. Wang, et al., Visualization and analysis of single-cell RNA-seq data by kernel-based similarity learning, Nat. Methods 14 (4) (2017) 414–416.
- [26] L. Zelnik-Manor, P. Perona, Self-tuning spectral clustering. Advances in Neural Information Processing Systems, 2004, p. 17.
- [27] L. Van der Maaten, G. Hinton, Visualizing data using t-SNE, Journal of machine learning research 9 (11) (2008).
- [28] D.L. Davies, D.W. Bouldin, A cluster separation measure. IEEE Transactions On Pattern Analysis and Machine Intelligence, 1979, pp. 224–227.
- [29] P.J. Rousseeuw, Silhouettes: a graphical aid to the interpretation and validation of cluster analysis, J. Comput. Appl. Math. 20 (1987) 53–65.
- [30] M.K. Pakhira, S. Bandyopadhyay, U. Maulik, Validity index for crisp and fuzzy clusters, Pattern. Recognit. 37 (3) (2004) 487–501.
- [31] S. Ray, R.H. Turi, Determination of number of clusters in k-means clustering and application in colour image segmentation, in: Proceedings of the 4th international conference on advances in pattern recognition and digital techniques, 1999. Calcutta. India.
- [32] A.E. Blanken, et al., Disentangling heterogeneity in Alzheimer's disease: Two empirically-derived subtypes, Journal of Alzheimer's Disease 70 (1) (2019) 227-239
- [33] M. Jové, et al., The causal role of lipoxidative damage in mitochondrial bioenergetic dysfunction linked to Alzheimer's disease pathology, Life 11 (5) (2021) 388.
- [34] J.H. Morra, et al., Automated mapping of hippocampal atrophy in 1-year repeat MRI data from 490 subjects with Alzheimer's disease, mild cognitive impairment, and elderly controls, Neuroimage 45 (1) (2009) S3–S15.
- [35] S.G. Costafreda, et al., Automated hippocampal shape analysis predicts the onset of dementia in mild cognitive impairment, Neuroimage 56 (1) (2011) 212–219.
- [36] L. Younes, et al., Inferring changepoint times of medial temporal lobe morphometric change in preclinical Alzheimer's disease, NeuroImage: Clinical 5 (2014) 178–187.
- [37] M. Deppe, et al., Increased cortical curvature reflects white matter atrophy in individual patients with early multiple sclerosis, NeuroImage: Clinical 6 (2014) 475–487.
- [38] J.B. King, M.P. Lopez-Larson, D.A. Yurgelun-Todd, Mean cortical curvature reflects cytoarchitecture restructuring in mild traumatic brain injury, NeuroImage: Clinical 11 (2016) 81–89.
- [39] P.A. Donnelly-Kehoe, et al., Looking for Alzheimer's Disease morphometric signatures using machine learning techniques, J. Neurosci. Methods 302 (2018) 24–34.

- [40] A.K. Lebedeva, et al., MRI-based classification models in prediction of mild cognitive impairment and dementia in late-life depression, Front. Aging Neurosci. (2017) 13
- [41] D. Murphy, et al., Volumetric magnetic resonance imaging in men with dementia of the Alzheimer type: correlations with disease severity, Biol. Psychiatry 34 (9) (1993) 612–621.
- [42] M.d.C. Valdés Hernández, et al., Do 2-year changes in superior frontal gyrus and global brain atrophy affect cognition? Alzheimer's & Dementia: Diagnosis, Assessment & Disease Monitoring 10 (1) (2018) 706–716.
- [43] E.C. Edmonds, et al., Heterogeneous cortical atrophy patterns in MCI not captured by conventional diagnostic criteria, Neurology. 87 (20) (2016) 2108–2116.
- [44] H.J. Lee, et al., Identification of heterogeneous subtypes of mild cognitive impairment using cluster analyses based on PET imaging of tau and astrogliosis, Front. Aging Neurosci. 12 (2021) 615467.
- [45] H. Braak, E. Braak, Neuropathological stageing of Alzheimer-related changes, Acta Neuropathol. 82 (4) (1991) 239–259.
- [46] J.L. Whitwell, et al., Neuroimaging correlates of pathologically defined subtypes of Alzheimer's disease: a case-control study, Lancet Neurol. 11 (10) (2012) 868–877.
- [47] J.L. Whitwell, et al., [18F] AV-1451 clustering of entorhinal and cortical uptake in Alzheimer's disease, Ann. Neurol. 83 (2) (2018) 248–257.
- [48] V.J. Lowe, et al., Widespread brain tau and its association with ageing, Braak stage and Alzheimer's dementia, Brain 141 (1) (2018) 271–287.
- [49] X. Sui, J.C. Rajapakse, A.S.D.N. Initiative, Profiling heterogeneity of Alzheimer's disease using white-matter impairment factors, NeuroImage: Clinical 20 (2018) 1222–1232
- [50] S.C. Verfaillie, et al., Thinner temporal and parietal cortex is related to incident clinical progression to dementia in patients with subjective cognitive decline, Alzheimer's & Dementia: Diagnosis, Assessment & Disease Monitoring 5 (2016) 43-52
- [51] D. Weintraub, et al., Alzheimer's disease pattern of brain atrophy predicts cognitive decline in Parkinson's disease, Brain 135 (1) (2012) 170–180.
- [52] A.A. Ali, et al., [P4–558]: Impact of alzheimer's disease development on the heart: focus on influence of physical and mental activity against the deleterious effect of social isolation and protein malnutrition, Alzheimer's & Dementia 13 (7S Part 32) (2017) P1566. -P1566.
- [53] N.P. Samant, G.L. Gupta, Adiponectin: a potential target for obesity-associated Alzheimer's disease, Metab. Brain Dis. 36 (7) (2021) 1565–1572.
- [54] J.A. Flores-Cordero, et al., Obesity as a risk factor for dementia and Alzheimer's disease: the role of leptin, Int. J. Mol. Sci. 23 (9) (2022) 5202.
- [55] P. Vemula, et al., Altered brain arginine metabolism in a mouse model of tauopathy, Amino Acids. 51 (2019) 513–528.
- [56] R.C. Eldridge, et al., Multiomics analysis of structural magnetic resonance imaging of the brain and cerebrospinal fluid metabolomics in cognitively normal and impaired adults, Front. Aging Neurosci. 13 (2022) 997.
- [57] M. Maitre, et al., Tryptophan metabolites modify brain Aβ peptide degradation: A role in Alzheimer's disease? Prog. Neurobiol. 190 (2020) 101800.
- [58] K. Savonije, D.F. Weaver, The Role of Tryptophan Metabolism in Alzheimer's Disease, Brain Sci. 13 (2) (2023) 292.
- [59] Y. Dong, et al., Essential protective role of tumor necrosis factor receptor 2 in neurodegeneration, Proceedings of the National Academy of Sciences 113 (43) (2016) 12304–12309.
- [60] Hooijsma, A., Targeting TNFR2 in Alzheimer's Disease. 2021.

[61] M. Amidfar, et al., The role of CREB and BDNF in neurobiology and treatment of Alzheimer's disease, Life Sci. 257 (2020) 118020.

Brain Multiphysics 6 (2024) 100093

- [62] S. Arora, T. Kanekiyo, J. Singh, Functionalized nanoparticles for brain targeted BDNF gene therapy to rescue Alzheimer's disease pathology in transgenic mouse model, Int. J. Biol. Macromol. 208 (2022) 901–911.
- [63] H. Svobodová, et al., Elevated Age-Related Cortical Iron, Ferritin and Amyloid Plaques in APPswe/PS1ΔE9 Transgenic Mouse Model of Alzheimer's Disease, Physiol. Res. 68 (2019) S445–S451.
- [64] M. Dulewicz, et al., Fatty Acid Binding Protein 3 (FABP3) and Apolipoprotein E4 (ApoE4) as lipid metabolism-related biomarkers of Alzheimer's disease, J. Clin. Med. 10 (14) (2021) 3009.
- [65] K.S. Lee, et al., Bioplex analysis of plasma cytokines in Alzheimer's disease and mild cognitive impairment, Immunol. Lett. 121 (2) (2008) 105–109.
- [66] F. Gongora-Rivera, et al., Chemokine profile in Alzheimer's disease: Results from a Mexican population, Journal of Clinical Neuroscience 73 (2020) 159–161.
- [67] J. Huang, et al., Inflammatory diseases, inflammatory biomarkers, and alzheimer disease: an observational analysis and mendelian randomization, Neurology. 100 (6) (2023) e568–e581.
- [68] Huang, J., B. Su, and V. Karhunen, Inflammatory Diseases, Inflammatory Biomarkers, and Alzheimer Disease.
- [69] G.E. Ennis, et al., Long-term cortisol measures predict Alzheimer disease risk, Neurology. 88 (4) (2017) 371–378.
- [70] J.G. Csernansky, et al., Plasma cortisol and progression of dementia in subjects with Alzheimer-type dementia, American Journal of Psychiatry 163 (12) (2006) 2164–2169.
- [71] N. Mattsson, et al., Association between longitudinal plasma neurofilament light and neurodegeneration in patients with Alzheimer disease, JAMa Neurol. 76 (7) (2019) 791–799.
- [72] Y.S. Lin, et al., Levels of plasma neurofilament light chain and cognitive function in patients with Alzheimer or Parkinson disease, Sci. Rep. 8 (1) (2018) 1–8.
- [73] L.J. Zhao, et al., Associations of the cerebrospinal fluid hepatocyte growth factor with Alzheimer's disease pathology and cognitive function, BMC. Neurol. 21 (1) (2021) 1-9.
- [74] Y. Zhu, et al., Serum hepatocyte growth factor is associated with small vessel disease in Alzheimer's dementia, Front. Aging Neurosci. 10 (2018) 8.
- [75] J.W. Wright, J.W. Harding, The brain hepatocyte growth Factor/c-Met receptor system: A new target for the treatment of Alzheimer's disease, Journal of Alzheimer's Disease 45 (4) (2015) 985–1000.
- [76] J. Wright, J.W. Harding, Small molecule activation of the neurotrophic hepatocyte growth factor to treat Alzheimer disease, Neuroimmunol. Neuroinflamm. 8 (2) (2021) 70–80.
- [77] R.M. Corbo, R. Businaro, D. Scarabino, Leukocyte telomere length and plasma interleukin-1β and interleukin-18 levels in mild cognitive impairment and Alzheimer's disease: new biomarkers for diagnosis and disease progression? Neural Regen, Res. 16 (7) (2021) 1397.
- [78] S.E. O'Bryant, et al., A blood screening test for Alzheimer's disease, Alzheimer's & Dementia: Diagnosis, Assessment & Disease Monitoring 3 (2016) 83–90.
- [79] H. Zetterberg, K. Blennow, Blood biomarkers: democratizing Alzheimer's diagnostics, Neuron, 106 (6) (2020) 881–883.
- [80] S.E. Schindler, et al., Using Alzheimer's disease blood tests to accelerate clinical trial enrollment, Alzheimer's & Dementia 19 (4) (2023) 1175–1183.